ISSN 1027-4510, Journal of Surface Investigation: X-ray, Synchrotron and Neutron Techniques, 2017, Vol. 11, No. 4, pp. 872–878. © Pleiades Publishing, Ltd., 2017.
Original Russian Text © V.B. Pikulev, D.V. Loginov, S.V. Loginova, 2017, published in Poverkhnost', 2017, No. 8, pp. 95–102.

Effect of the Carbon Component on the Electrical and Optical Properties of Nanocellulose-Based Composites

V. B. Pikulev, D. V. Loginov, and S. V. Loginova*

Petrozavodsk State University, Petrozavodsk, 185910 Republic of Karelia, Russia

**e-mail: logindm@mail.ru*

Received November 30, 2016

Abstract—The results of X-ray studies of the structure of components of composite materials based on milled microcrystalline cellulose are presented. The 3D model of the atomic arrangement in the short-range order of amorphous carbon can be described by a mechanical mixture of two types of clusters in the ratio of 1 : 2. One type of clusters is formed by two planar graphene single layers shifted relative to each other and containing vacancies, and the other type is presented by six graphene grids. The cellulose matrix with silicon nanoparticles has a low photoluminescence-signal degradation rate. The introduction of fullerenes into nanomaterial as a third nanofraction, as well as the action of ozone, leads to anomalous luminescence kinetics under UV (ultraviolet) photoexcitation, which can be associated with competing processes of hydrogen and oxygen adsorption on the surface of silicon nanoparticles. A change in the ionic conductivity of the porous cellulose matrix upon exposure to ozone can be used to develop effective ozone detectors. Such a filler as amorphous-crystalline carbon causes not only ionic but also electronic conductivity in the sample; however, the processes of space-charge redistribution remain dependent only on the ion-current component. An increase in the total current passing through the pressed sample eliminates the need for a further increase in the signal in the design of ozone sensors.

Keywords: nanocomposite, cellulose, fullerenes, amorphous carbon, photoluminescence, ionic and electronic conductivity

DOI: 10.1134/S1027451017040267

INTRODUCTION

Cellulose-based composites are a very promising object of modern research [1]. The composite material, the structure and properties of which are discussed in this paper, has photoluminescence with a maximum at 1.8–1.9 eV, caused by well-known quantum-size effects in silicon nanoparticles [2], which was confirmed in [3, 4]. A porous cellulose matrix is a medium capable not only of retaining spatially separated silicon nanoparticles but also of ensuring the flow of hydrogen atoms to their surface, as water can form stable crystallization compounds with cellulose molecules [5]. It is assumed that passivation of the surface of silicon nanoparticles with hydrogen can be a condition for stabilization of the quantum efficiency of photoluminescence, which determines a higher degradation resistance of the composite luminescence as compared to the same silicon nanoparticles on a dielectric substrate under atmospheric conditions. The reason for the degradation of luminescence in the latter case is the effect of oxidation of the composite, primarily, due to the action of active (singlet) oxygen [6].

The possibility of generating singlet oxygen by using C_{60} fullerenes excited in the intrinsic absorption band has been demonstrated [7]. The creation of a composite containing both silicon nanoparticles and fullerenes in a cellulose matrix suggests the appearance of opposing factors affecting the intensity of the luminescence signal.

The transfer of electric charges in a cellulose matrix under normal conditions is usually related to ionic conductivity phenomena [8], which is sufficient evidence of the presence of protons freely moving in the cellulose matrix.

We show that the external action of ozone, which stimulates degradation of the luminescence signal, affects the magnitude of the ion current [9]. The presence of a carbon component with electronic conductivity makes it possible to compare the behavior of the electron and ion currents flowing in the composite.

EXPERIMENTAL

Microcrystalline cellulose, further subjected to ultrasonic dispersion in distilled water, followed by its evaporation, was used as a cellulose matrix for the nanocomposite. The source of silicon single crystals was silicon powder prepared by the mechanical and ultrasonic dispersion of porous silicon in a solution of isopropanol. The initial porous silicon was prepared

Table 1. Investigated three-component nanocomposites

Material	Composition	Method of preparation
Composite no. 1	Nanosilicon + NC + extract of fullerenes (mixture)	Compressed tablet
Composite no. 1c		Suspension
Composite no. 2	Nanosilicon + NC + amorphous carbon (carbon black)	Compressed tablet

by the electrochemical etching of a KDB-1 single-crystal silicon wafer in an alcoholic (1 : 1 vol %) solution of 40% hydrofluoric acid [3, 4].

A sample (mixture) of fullerenes was obtained by the high-temperature treatment of graphite; the mixture of fullerenes was separated from the graphite component with organic solvents, after which further chromatic separation took place. Amorphous carbon powder was obtained in electric arc plasma with graphite electrodes in helium.

The fractional composition of the composites presented in Table 1 was the same: the ratio of the volume parts of nanosilicon, carbon powder, and cellulose was 1 : 1 : 30, respectively. Each component was diluted in the same amount of solvent (tetrachloroethane was used for carbon-containing powders, and isopropanol was used for the others); then all three parts were mixed. The light fraction containing no tetrachloroethane was separated for use and dispersed for 30 min in an ultrasonic bath. The resulting suspension was poured into a Petri dish, where the solvent was evaporated at room temperature. As a result, a light gray substance was obtained from which tablets were formed by pressing at a pressure of 0.26 MPa. The color of the resulting tablets ranged from light brown to black.

RESULTS AND DISCUSSION

The structural state of the constituents of the three-component system was studied and controlled by X-ray methods. X-ray diffraction measurements of the powders of porous silicon and nanocellulose were carried out using a DRON-6.0 automated diffractometer with CuK_α radiation in the angular range from 3° to 145° in the symmetric reflection and transmission geometry.

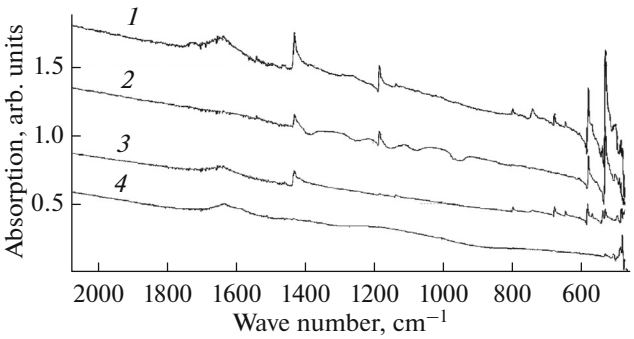

Fig. 1. IR spectra of carbon components of the NCC nanocomposite under study: (*1*) mixture of fullerenes (C_{60}, 71.31%; C_{70}, 22.29%; C_{76}, 3.05%; C_{84}, 1.90%, and impurities, less than 1%), (*2*) powder of pure fullerenes C_{60}, (*3*) powder of pure fullerenes C_{70}, and (*4*) powder of amorphous carbon.

The degree of crystallinity used to create a composite of nanocrystalline cellulose, calculated by the method of [10], was 60 ± 5%. The dimensions of the coherent scattering regions of nanostructured cellulose take different values depending on the crystallographic direction: the minimum size in the direction [$\bar{1}$10] is 40 ± 5 Å, and the maximum one in the direction [001] is 70 ± 5 Å. The thickness and length of elementary fibrils in the material are approximately 50 and 70 Å, respectively [3, 4].

It was shown earlier that X-ray diffraction patterns of the nanocomposite samples based on nanocrystalline cellulose (NCC) with a crystallinity of 77% show an increase in the amorphous component by 20% [3]. This can be explained by the fact that some of the silicon nanocrystals are embedded in the cellulose matrix. A similar increase in the X-ray diffraction patterns of samples based on NCC with a crystallinity of 60% is not observed. It is likely that an increase in the amorphous phase and, consequently, an increase in the number of sites with a disordered arrangement of cellulose macromolecules in the sample make it possible to incorporate porous silicon particles into the cellulose matrix without noticeable changes in the X-ray image [11].

The distribution curves of the scattering intensity of the samples of carbon components were obtained using a DRON-6.0 diffractometer with CuK_α and MoK_α radiation in the transmission and reflection geometry.

In Fig. 1, the IR absorption curves *1* and *4* correspond to the carbon powders used in the work (Table 1), and curves *2* and *3* are given for comparison.

The distribution curves of the scattering intensity $I(2\theta)$ of a two-component nanocomposite, composite no. 1 (with the fullerene extract), the fullerene extract, and X-ray diffraction patterns for fullerites C_{60} and C_{70}, calculated theoretically according to the data of [12, 13], are given for comparison (Fig. 2).

The X-ray diffraction pattern of the composite (curve *2*) contains slight traces of reflections from fullerites C_{60} and C_{70}. On the distribution curve of the intensity of scattering by the fullerene extract (curve *3*),

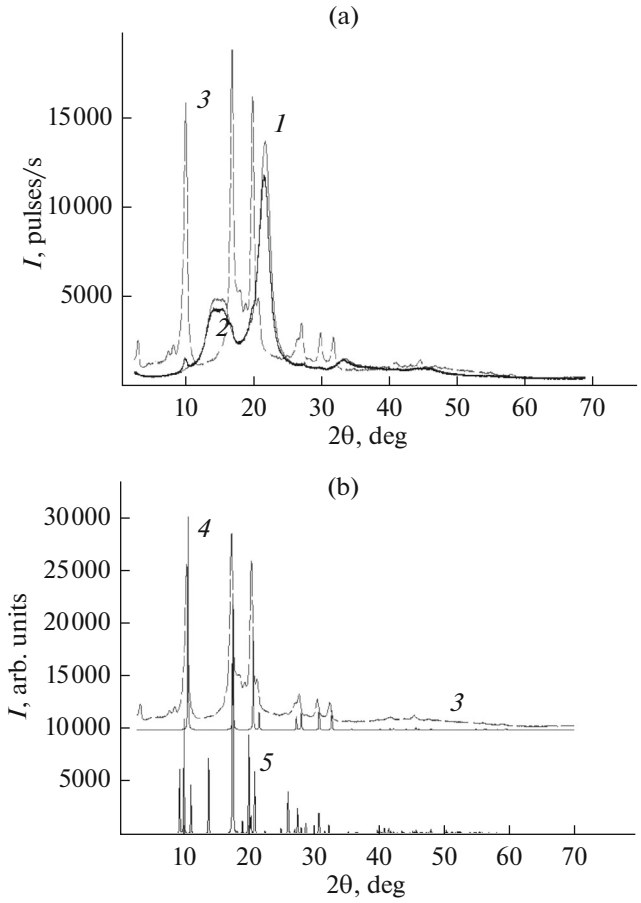

Fig. 2. Scattering intensity distribution curves of (a) (*1*) two-component nanocomposite, (*2*) composite no. 1, and (*3*) fullerene extract and (b) (*3*) fullerene extract and curves theoretically calculated for (*4*) C_{60} and (*5*) C_{70} fullerites.

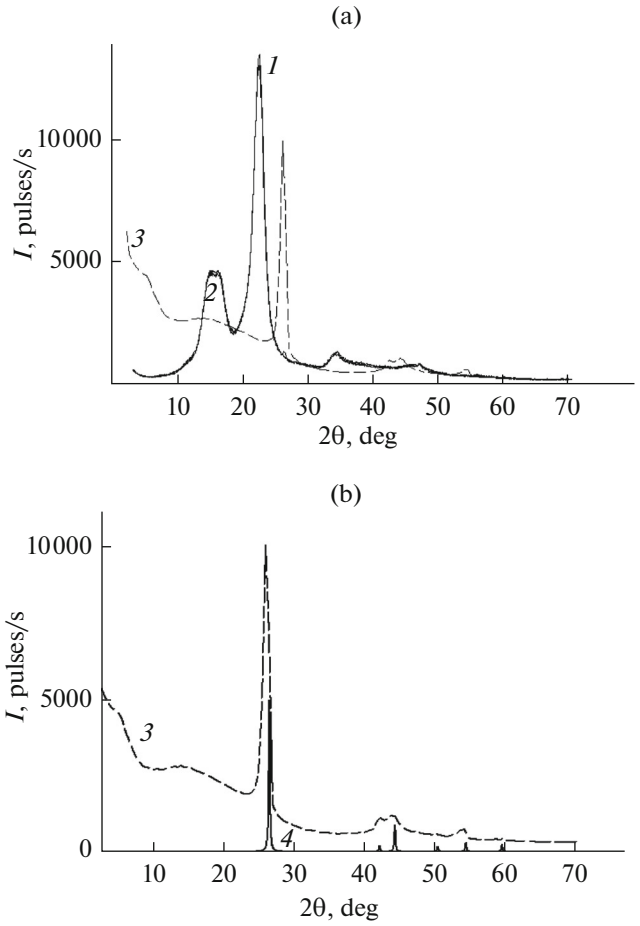

Fig. 3. Scattering intensity distribution curves of (a) (*1*) two-component nanocomposite, (*2*) composite no. 2, and (*3*) carbon powder and (b) (*3*) carbon powder and curve theoretically calculated for (*4*) hexagonal graphite JCPDS 41-1487.

there are reflections of higher fullerenes in addition to reflections from the above fullerites.

The X-ray diffraction patterns of a two-component nanocomposite, nanocomposite no. 2, and carbon powder and a theoretically calculated X-ray diffraction pattern of hexagonal graphite (JCPDS 41-1487) are shown for comparison in Fig. 3. In the experimental distribution curve of the scattering intensity of nanocomposite no. 2 (curve *2*), there is a weak reflection corresponding to the X-ray line from the base plane (002) of hexagonal graphite.

The X-ray diffraction pattern of the carbon powder (curve *3*) shows a characteristic diffuse halo corresponding to amorphous carbon [14] and a reflection from hexagonal graphite (~26.2°), shifted toward smaller scattering angles. This maximum characterizing scattering at a packet of graphene grids is shifted toward smaller scattering angles. Such a shift was observed in [14, 15] for carbon materials of natural and synthetic origin. The interlayer distance calculated from the position of line (002) is 3.39Å. In the curve of the $I(2\theta)$ dependence of the carbon powder, there is a maximum in the region of 5° and a diffuse maximum in the angular range from 8° to 23°.

The characteristics of the short-range order of amorphous carbon were calculated using the Finbak–Warren method [16]. Corrections for scattering at air, polarization, and absorption were introduced into the experimental scattering intensity distribution curves. The *s*-weighted interference functions $H(s)$ and the distribution curves of the pair functions were calculated, from which the quantitative characteristics of short-range order (the radii of the coordination spheres and their blurring; coordination numbers) were calculated [16]. The results of calculating the short-range order characteristics for the carbon powder are given in the Table in comparison with the data for hexagonal graphite.

The radii of the first three coordination spheres of graphite and the powder under study differ. This is especially true for the radius of the 3rd coordination sphere of C–C, which in the sample under study is

Table 2. Radii r_i and degradation σ_i of the coordination spheres and coordination numbers N_i calculated for amorphous carbon and hexagonal graphite

No. of sphere	Hexagonal graphite		Carbon powder		
	$\langle r_i \rangle$, Å	$\langle N_i \rangle$, at	r_i, Å	σ_i, Å	N_i, at
1	1.42	3.0	1.44	0.19	2.8 ± 0.1
2	2.46	6.0	2.43	0.06	4.0 ± 0.1
3	2.84	3.0	2.78	0.30	5.2 ± 0.2
4	3.35	1.0	3.30	0.00	0.8 ± 0.1
5	3.68	15.0	3.75	0.22	10.1 ± 0.3
6	4.27	21.0	4.26	0.25	11.6 ± 0.4
7	5.01	30.0	4.99	0.40	27.4 ± 0.3
8	5.41	6.0	5.41	0.35	2.5 ± 0.5
9	5.67	3.0	5.72	0.28	15.1 ± 0.5
10	6.08	30.0	6.13	0.14	14.2 ± 0.7
11	6.57	26.0	6.50	0.18	18. 3 ± 0.8
12	7.06	36.0	7.00	0.3	31.2 ± 0.8
13	7.31	24.0	7.31	0.28	13.7 ± 1

0.06 Å smaller than that in hexagonal graphite. The reason for the decrease in this distance in amorphous carbon is probably the presence of vacancies in carbon grids, as evidenced by the underestimated coordination number on the 2nd coordination sphere.

The intergrid distance (the radius of the 4th coordination sphere) is underestimated by 0.05 Å compared to the same distance for graphite. The number of carbon atoms in this sphere is the same, within experimental error, as the number of carbon atoms in graphite. The radius of the 11th coordination sphere, corresponding to the second intergrid distance, is lowered by 0.07 compared to that for graphite. The coordination number in this sphere is lowered by approximately 30%. The radii of the 5th and 12th coordination spheres differ from the values for hexagonal graphite by 0.07 Å: the radius of the 12th sphere is underestimated, while the radius of the 5th sphere is overestimated. The radii of the 6th, 7th, 8th, and 13th spheres correspond to the values calculated for graphite. The radii of the 9th and 10th coordination spheres are larger than the corresponding values for graphite by 0.05 Å.

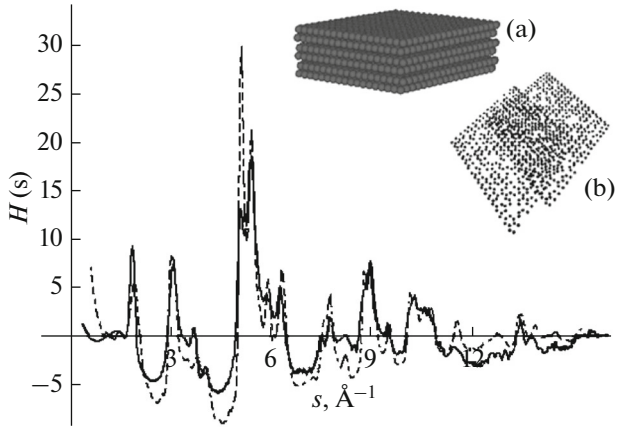

Fig. 4. Curves of interference *s*-weighted functions: (solid line) composite no. 2 and (dashed line) curve theoretically calculated for a mechanical mixture of clusters. The inset shows: (a) a cluster of hexagonal graphite and (b) a cluster consisting of two carbon planes shifted relative to each other and having vacancies.

Thus, the values of the radii of the coordination spheres and the coordination numbers in the sample of amorphous carbon powder differ from the corresponding values for hexagonal graphite. To characterize the arrangement of atoms in the short-range order regions, spatial atomic configurations were constructed by the method described in [17]. For all spatial models constructed, consisting of planar or curved layers of graphene, the scattering intensity distribution curves and *s*-weighted interference functions were plotted and were compared with the corresponding experimental curves. The lowest value of the uncertainty factor (26%) in comparing the experimental and model $H(s)$ curves was obtained for a model that is a mechanical mixture of clusters of two types: one is clusters of hexagonal graphite consisting of six graphene layers with the dimensions $18a \times 18b$, where a and b are the periods of the unit cell of hexagonal graphite (Fig. 4, see inset a), and the other is clusters consisting of two carbon planes measuring $18a \times 18b$, displaced by 25 Å relative to each other, and containing 280 vacancies with a total number of atoms of 1296 (Fig. 4, see inset b). Calculation of the theoretical curves of *s*-weighted interference functions with a different percentage of clusters of the former and latter types showed that the best agreement is achieved in the case of the cluster ratio of 1 : 2 (Fig. 4).

It should be noted that there is no increase in the diffuse maximum on the X-ray diffraction patterns of nanocomposites nos. 1 and 2, as compared to the maximum in curve $I(2\theta)$ of NCC.

The luminescence kinetics of composite no. 1 (containing fullerenes and silicon nanoparticles) recorded under prolonged action of the excitation radiation of a He–Cd laser with a wavelength of 325 nm is shown in Fig. 5 (curve *1*). For comparison, the curve of degradation of silicon nanoparticles in air under similar excitation conditions is given (curve *2*). In the latter case, the luminescence signal of the fullerene-containing composites decreases with prolonged exposure to UV radiation, which is well approximated by a stretched exponent. Such kinetics is due to oxidation processes occurring on the surface of silicon nanocrystallites, leading to an increase in the number of defects on the surface of silicon crystallites, which

play the role of nonradiative recombination centers. Curve *1*, in contrast, shows an increase in the luminescence intensity with a further weak tendency to a decreasing signal.

The results can be interpreted as follows. On the one hand, ultraviolet radiation should lead to the generation of singlet oxygen in fullerene molecules. The access of oxygen to the porous samples of the composite can occur at any depth, and some degradation of luminescence upon exposure to ozone (Fig. 6, curves *1*–*3*) is confirmation of this. At the same time, ultraviolet radiation in the presence of active oxygen leads to the destruction of cellulose molecules [18], which enables hydrogen to be released as atoms or ions. The presence of water in the pores of the cellulose matrix also forms additional sources of hydrogen generation. Thus, there is a competing mechanism of change in the passivation of the surface of silicon crystallites, stimulated by ultraviolet irradiation. However, when the silicon coating is replaced with hydrogen, surface defects decrease, which blocks the nonradiative recombination channel over surface defects, and as a result, the luminescence signal is amplified.

IR spectroscopy data show an increase in the amount of OH groups (in the region of 3000–3500 cm^{-1}) with prolonged laser excitation, but the position of the absorption peak of silicon oxide is completely masked by intense absorption peaks of cellulose (800 to 1300 cm^{-1}), which does not enable estimation of the magnitude of the change in the oxide phase of silicon from the shape of the IR spectra. Saturation of the composite with water molecules leads to a noticeable increase in the luminescence intensity by a maximum of 1.5 times (Fig. 6, see inset). This suggests that water bound in the cellulose matrix plays an important role in the mechanism of the suppression of nonradiative recombination during excitation relaxation in silicon nanoparticles.

The study of charge transfer in composites based on a cellulose matrix was carried out in a well-shielded chamber of the vacuum installation, which made it possible to investigate currents in the range of picoampere units in vacuum, under atmospheric conditions, and when ozone was supplied. The contacts to the opposite sides of the samples (compressed tablets) were formed by an indium–gallium eutectic or perforated copper plates to conduct experiments with the supply of gases to the sample.

Figure 7 presents the sequence of kinetics of the change in the discharge current of a sample previously polarized at a voltage of 64 V. Kinetic measurements were carried out at room temperature. The ballast resistance was 100 MΩ. The obtained dependences indicate the redistribution of slow mobile charges in matter against the background of much lower values of the direct current flowing through the sample. The kinetics of the change in the potential is asymmetric for different polarities, and with each cycle of potential

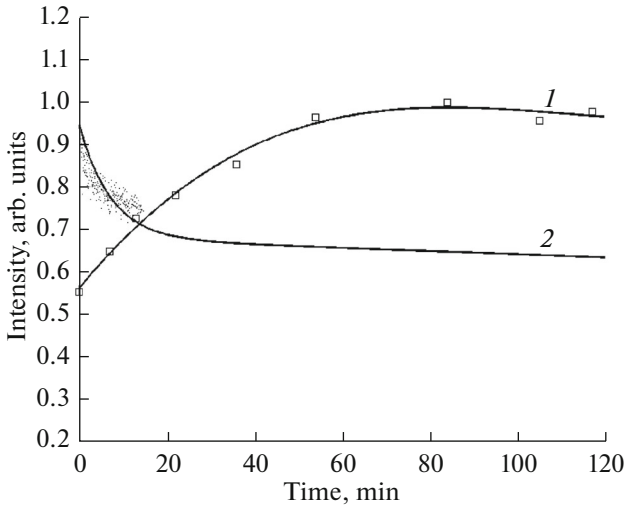

Fig. 5. Kinetics of the intensity of the luminescence signal for (*1*) composite no. 1 and (*2*) silicon nanoparticles; points are experimental values.

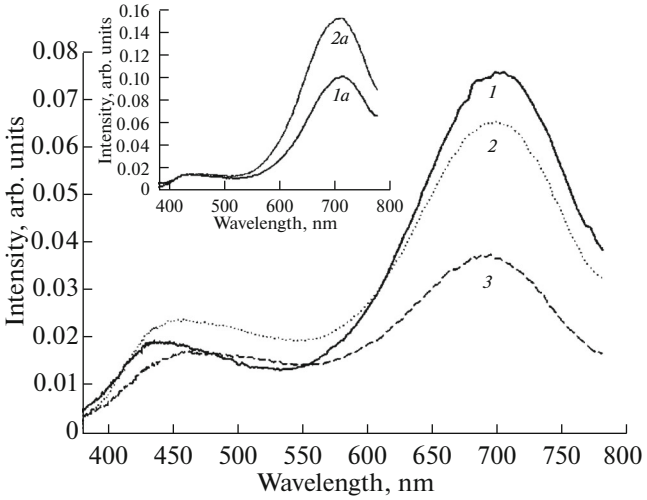

Fig. 6. Photoluminescence of nanocomposite no. 1c, deposited onto a silicon substrate under the effect of ozone and water: (*1*) initial state of the sample and after (*2*) 5 and (*3*) 15 min of ozone exposure. The inset shows a similar sample, subjected to a single treatment with water ((*1a*) before exposure and (*2a*) after exposure).

change, there is an increase in both the discharge current and the initial potential difference.

When the temperature of the composite, which is devoid of the carbon component, is lowered to the temperature of liquid nitrogen, the current through the sample becomes zero, and charge transfer is impossible. Starting from a temperature of about 220–260 K, a potential difference appears (corresponding to the polarity of the preliminarily charged sample), which increases in magnitude with increasing sample temperature. For a composite with amorphous car-

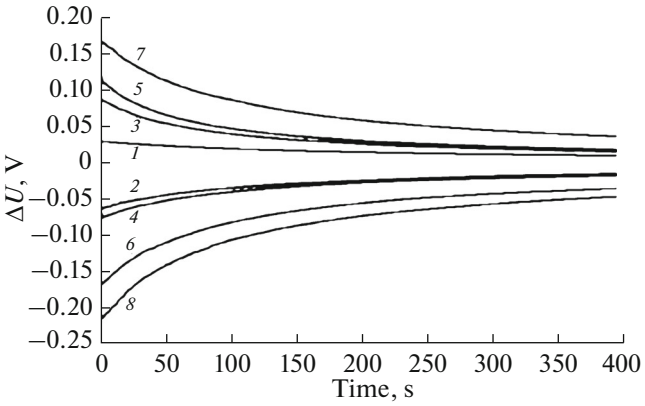

Fig. 7. Kinetics of the potential drop at the contacts of nanocomposite no. 2 for a series of consecutive 10-min recharges with a change in the polarity of the applied voltage (64 V): (*1*) after the first charge, (*2*) after three 10-min charging cycles with a change in polarity, and (*3*–*8*) after subsequent recharge cycles.

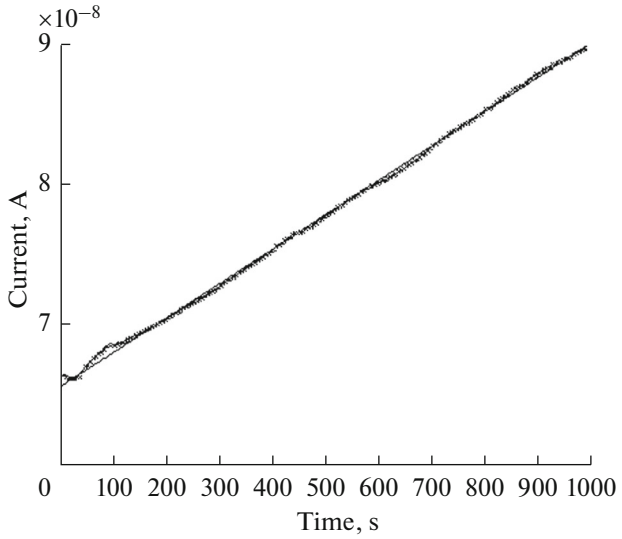

Fig. 8. Effect of ozone on the kinetics of the current in composite no. 2 at a voltage of 25 V: points are the experiment and the curve is the approximation.

bon, a relatively weak current of 1.3 μA was recorded at 77 K.

Thus, the hypothesis of an ionic mechanism of charge transport in the given substance seems most correct in describing the charge transfer in a nanocomposite [8, 19]. At the temperature of liquid nitrogen, the ion transport velocity decreases substantially, which is manifested in the absence of the possibility of charge exchange and restoration of the potential difference at the contacts. The presence of silicon nanoparticles, apparently, does not affect the flow of electron and ion currents in the composite, nor does the flow of currents in the sample affect its luminescence properties. The increase in current with each new charge-exchange cycle of the sample (Fig. 7) may be due to the peculiarities of the movement of hydronium ions along the grid of water bridges. We can assume that the effect of an external electric field not only leads to the movement of these ions, but also changes the orientation of cellulose whiskers [20], gradually forming a more ordered network of current channels.

The effect of a constant-concentration ozone flux (5 mg/min) on current flowing through a composite tablet with a filler in the form of amorphous carbon is presented in Fig. 8. Just as in the absence of a carbon component in a composite based on nanostructured cellulose, there is a tendency for a linear increase in the current density from the time of exposure [9]. However, in this case, the current is higher by one and a half orders of magnitude, which reduces the requirements for the amplifying device when creating the ozone-detector prototype.

The mechanism of the presented effect is not completely understood. Obviously, ozone, like singlet oxygen, due to its exceptionally high chemical activity, should stimulate proton-exchange reactions in a cellulose matrix, leading ultimately to an increase in the number of mobile hydrogen ions. At the same time, an increase in the number of OH groups in the IR spectra with the corresponding ozone effect was not reliably recorded in our experiments.

CONCLUSIONS

Thus, the samples under investigation have luminescence in the red region of the visible spectrum, similar to the luminescence of porous silicon. A distinctive feature of the new material from systems of "porous silicon–fullerenes" is that there is no self-oxidation of the composite under the action of ultraviolet radiation in the presence of fullerenes. This fact explains the anomalous behavior of the photoluminescence degradation kinetics, which shows a much higher degradation resistance of the luminescence signal in three-component nanocomposites during photoexcitation under normal conditions. This effect can be caused by the gradual "healing" of defects on the surface of silicon nanocrystallites with the formation of stable hydrogen passivation due to photostimulated desorption and adsorption reactions on the surface of silicon nanoparticles.

The electronic and ionic conductivity type is characteristic of a composite containing amorphous carbon as a third component. In such a composite, the processes of the redistribution of space charge are determined exclusively by the ionic component of the current. A change in the ionic conductivity of the porous cellulose matrix upon exposure to ozone can be used to develop effective ozone detectors.

The resulting nanocomposite has a glow homogeneous in volume; in the form of a solution, it can fill

regions of any profile and be subjected to compression and mixing with other substances. One possible application of the new material is its use as an invisible luminescent and electric tag for identifying paper documents.

ACKNOWLEDGMENTS

The research was supported by the strategic development program "University Complex of Petrozavodsk State University in the Scientific and Educational Space of the European North: the Strategy of Innovative Development" for 2012–2016.

REFERENCES

1. J. Hinestroza and A. N. Netravali, *Cellulose Based Composites: New Green Nanomaterials* (Wiley, New York, 2014).
2. V. Kumar, *Nanosilicon* (Elsevier, Amsterdam, 2007).
3. V. Pikulev, S. Loginova, and V. Gurtov, Nanoscale Res. Lett. **7**, 426 (2012).
4. V. B. Pikulev, S. V. Loginova, and V. A. Gurtov, Tech. Phys. Lett. **38** (8), 723 (2012).
5. E. A. Kolosovskaya, S. R. Loskutov, and B. S. Chudinov, *Physical Foundations of Interaction between Wood and Water* (Nauka, Novosibirsk, 1989) [in Russian].
6. D. Kovalev, E. Gross, J. Diener, et al., Appl. Phys. Lett. **85** (16), 3590 (2004).
7. A. Sienkiewicz, S. Garaj, E. Bialkowska-Jaworska and L. Forro, in *Electronic Properties of Novel Materials–Molecular Nanostructures,* Ed. by H. Kuzmany (American Institute of Physics, New York, 2000), p. 63.
8. M. Nilsson and M. Stromme, J. Phys. Chem. B **109**, 5450 (2005).
9. V. B. Pikulev, P. F. Prokopovich, and V. A. Gurtov, Uch. Zap. Petrozavodsk. Gos. Univ., No. 2 (148), 77 (2015).
10. N. Terinte, R. Ibbett, and K. C. Schuster, Lenzinger Ber. **89**, 118 (2011).
11. V. B. Pikulev, S. V. Loginova, and D. V. Loginov, Uch. Zap. Petrozavodsk. Gos. Univ., No. 8 (137), 110 (2013).
12. D. L. Dorset and M. P. McCourt, Acta Crystallogr., Sect. A: Found. Crystallogr. **50**, 344 (1994).
13. S. van Smaalen, V. Petricek, J. L. de Boer, et al., Chem. Phys. Lett. **223**, 323 (1994).
14. L. A. Aleshina, N. V. Melekh, and D. V. Loginov, *Some Promising Materials of North-West of the Russian Federation on the Base of Cellulose, Carbon and Silicates* (Petrozavodsk State Univ., Petrozavodsk, 2012) [in Russian].
15. K. Usenbaev, K. Zhumalieva, and Yu. Kalinin, Dokl. Akad. Nauk SSSR **232** (5), 1189 (1977).
16. L. A. Aleshina and S. V. Loginova, Crystallogr. Rep. **48** (4), 531 (2003).
17. L. A. Aleshina, D. V. Loginov, A. D. Fofanov, and R. N. Kyutt, Phys. Solid State **53** (8), 1739 (2011).
18. A. Potthast, T. Rosenau, and P. Kosma, Adv. Polym. Sci. **205**, 1 (2006).
19. M. Nilsson and M. Strømme, J. Phys. Chem. B **109**, 5450 (2005).
20. D. Bordel, J.-L. Putaux, and L. Heux, Langmuir **22**, 4899 (2006).

Translated by O. Zhukova